Available online at www.sciencedirect.com
SCIENCE DIRECT®
Journal of Non-Crystalline Solids 348 (2004) 162–171
JOURNAL OF NON-CRYSTALLINE SOLIDS
www.elsevier.com/locate/jnoncrysol

Preparation and characterization of cerium doped silica sol–gel coatings on glass and aluminum substrates

A. Pepe [a], M. Aparicio [b], S. Ceré [a], A. Durán [b,*]

[a] *INTEMA-Conicet., Av. J. B. Justo 4302, B7608FDQ Mar del Plata, Argentina*
[b] *Instituto de Cerámica y Vidrio. CSIC – Campus de Cantoblanco, 28049 Madrid, Spain*

Abstract

Chromates are among the most common substances used as corrosion inhibitors. However, these compounds are highly toxic, and an intense effort is being undertaken to replace them. Cerium compounds seem to fulfil the basic requirements for consideration as alternative corrosion inhibitors. The aim of this work was to study the effect of the incorporation of cerium ions in silica sol–gel coatings on aluminum alloys as potential replacement of chromate treatments. The main idea was to combine the 'barrier' effect of silica coatings with the 'corrosion inhibitor' effect of the cerium inside the coatings. Thin (below 1 μm for a single layer) and transparent cerium doped silica sol–gel coatings were prepared by dipping 3005 aluminum alloys in sol–gel solutions. Ultra-violet–visible spectra (UV–vis) show that cerium ions, Ce^{3+} and Ce^{4+}, always are present in the coatings, independently of the cerium salt or firing atmosphere used. Active protection with single and two layer coatings prepared with Ce (IV) salt seems to improve corrosion protection of the coated aluminum while coatings prepared with Ce(III) salt only entails a protection when applied as a two layer, possibly due to sealing of pre-existent defects in the first layer. The improvement of active protection with immersion time would imply that corrosion is inhibited by cerium ions that migrate through the coating to the site of the attack (a defect in the coatings) and then react to passivate the site.

1. Introduction

Aluminum alloys are widely used in different industry fields, owing their excellent corrosion resistance to the barrier oxide film strongly bonded to the surface. Aluminum alloy 3005 with Mn, Mg, Fe and Si as major alloying elements, is typically used on residential siding, mobile home sheet, gutters and downsports, sheet metal work, bottle caps and closures. The alloys of the series 3000 are resistant to uniform corrosion [1]. The manganese is present in the aluminum solid solution, in submicroscopic particles of precipitate and in larger particles of $Al_6(Mn,Fe)$ or $Al_{12}(Mn,Fe)_3Si$ phases [1,2], both of which have solution potentials almost the same as that of the solid solution matrix [1,2]. In general, the resistance of the 3000, 5000 and 6000 aluminum alloys to general corrosion are similar, and greater than that of 2000 and 7000 alloys [2]. However, their tendency to corrosion in the presence of halide ions limits their applications [1–3]. Corrosion of aluminum involves the adsorption of these ions on the surface, reaction of the anion (e.g. Cl^-) with aluminum in the oxide layer, thinning it by reaction/dissolution, and attack of the exposed metal [4].

One of the best strategies to improve the corrosion resistance is the use of coatings with the incorporation of corrosion inhibitors. Cr(VI) compounds, mainly chromates, are among the most common substances used, and their efficiency/cost ratio has made them standard corrosion inhibitors. Chromates have been applied in three different ways: incorporated into conversion

* Corresponding author. Tel.: +34 91 7355840; fax: +34 91 7355843.
E-mail address: aduran@icv.csic.es (A. Durán).

0022-3093/$ - see front matter © 2004 Elsevier B.V. All rights reserved.
doi:10.1016/j.jnoncrysol.2004.08.141

coatings, as an additive in anodizing baths and as pigment in painting primers [5]. However, these compounds are toxic [6], and an effort is being undertaken to replace them [6,7]. Cerium compounds seem to fulfil the basic requirements for consideration as alternative corrosion inhibitors: the ions form insoluble hydroxides which enable them to be used as cathodic inhibitors [6], they have a low toxicity [8,9], and are relatively abundant in nature [8,9].

Different authors [10–13] have studied the effect of immersing aluminum alloys in water solutions of cerium salts on both uniform and pitting corrosion. The kind of cerium salt, the concentration, and the immersion times have been also evaluated. Uniform and localized corrosion rates of a large variety of aluminum alloys decrease with the concentration of cerium salts. Cerium compounds have been classified as cathodic inhibitors taking into account the relative position of cathodic branches in the polarization diagrams that move down to more negatives values of potential [10]. Cerium has an affinity for oxygen [11], and the bonding between cerium and oxygen is unlikely to be broken under the cathodic applied potentials [11]. It was found [12,13] that, during deposition, hydrated cerium oxide initially covers the intermetallic compounds present on the aluminum alloy surface and then tends to cover the whole surface. The cathodic potential shift can be related to the formation of the layer formed by cerium oxide/hydroxide. Hinton proposed that when the oxygen reduction reaction occurs at activated cathodic site producing OH^- groups, the pH increases in the vicinity of the sites giving rise to the precipitation of $Ce(OH)_3$ [14–18].

One of the most technologically important aspects of sol–gel processing is the ability to prepare coatings with sintering temperatures lower than 500 °C. The preparation of coating by dipping substrates in sol–gel solutions is an established method to produce homogeneous coatings with uniform thickness below 2 μm [19]. Different sol–gel coatings have been developed to increase the corrosion resistance of metals, although the inorganic ones have limitations such as micro cracks, residual porosity and thickness limitations. The incorporation of organic groups, covalently attached to the silicon atom, reduces these limitations [19,20]. On the other hand, sol–gel materials provide a vehicle for the incorporation of secondary phases including metal ions and particles [21,22]. Cerium ions and other elements have been incorporated into sol–gel coatings for optical purposes [23–25].

The aim of this work was to study the effects of the incorporation of cerium ions in silica sol–gel coatings deposited onto aluminum alloys as potential replacement of chromate treatments. A semiquantitative evaluation of Ce^{3+}/Ce^{4+} ratio by UV–vis spectroscopy is performed to distinguish the effect of the oxidation state in the corrosion process. This system should combine the 'barrier protection' effect of silica coatings with the 'corrosion inhibitor' effect of the cerium ions inside the coatings. Silica coatings used as barriers prevent contact between the aluminum alloy surface and corrosive species. Active protection with cerium would imply that corrosion is inhibited by cerium ions that migrate through the coating to the site of the attack (a defect in the coatings) and then react to passivate the site.

2. Experimental

2.1. Preparation of sols

Solutions with 95Si–5Ce and 90Si–10Ce molar compositions were prepared by the sol–gel method through hydrolysis and polycondensation reactions. Tetraethylorthosilicate [$Si(OC_2H_5)_4$, TEOS], methyltriethoxysilane [$SiCH_3(OC_2H_5)_3$, MTES], both from ABCR, cerous nitrate [$Ce(NO_3)_3 \cdot 6H_2O$], and ammonium ceric nitrate [$Ce(NH_4)_2(NO_3)_6$], both from Aldrich, were used as starting materials.

Sols with the Ce(III) salt were prepared firstly dissolving the salt in absolute ethanol by agitation at 40 °C for 30 min. After that, calculated amounts of TEOS and MTES (molar ratio TEOS/MTES = 20/80), HNO_3 1 N and acetic acid (molar ratio water/acetic acid = 7) were added, stirring at 40 °C for 4 h. The final molar ratio water/TEOS + MTES was 2, with a sol concentration of 150 g of oxide per litre. Ammonium ceric nitrate is more difficult to dissolve. In this case, TEOS and MTES were mixed with HNO_3 1 N, acetic acid and ethanol, with the same molar ratios used above, stirring at 40 °C for 1 h. Then, the Ce(IV) salt was incorporated and dissolved by agitation at 40 °C for 3 h. The molar ratio water/TEOS + MTES was 2, and the final sol had a concentration of 100 g/l of oxides.

2.2. Substrates and coatings

Cerium doped silica sol–gel coatings were deposited on soda-lime glass slides and aluminum alloy 3005 substrates. Glass and aluminum samples ($4.5 \times 10\,cm^2$) were cleaned ultrasonically in ethanol for 5 min, and left in ethanol until the preparation of the coating. Coatings were obtained by dipping at room temperature in a glove box with a 7% of relative humidity, and a withdrawal rate of 28 cm/min. Coated glass substrates were treated at 450 °C for 15 min in three different atmospheres: air, nitrogen and 90%N_2–10%H_2, with the aim of studying the effect of atmosphere in the final oxidation state of cerium. The coatings on aluminum samples were prepared only with 90Si–10Ce sols from both cerium precursors, and treated in air at 450 °C for 15 min. Two layer coatings were prepared on aluminum substrates with a thermal treatment in air at 450 °C after each deposition process.

2.3. Characterization of gels and coatings

The coating thickness was measured on glass samples after densification by using a profilometer (Talystep, Taylor-Hobson, UK) on a scratch made immediately after deposition. Absorbance spectra of coatings on glass substrates were obtained with a UV–vis NIR spectrophotometer (Perkin–Elmer Lambda 9) with integrating sphere. An uncoated substrate was used as reference to obtain the spectra of coatings. The error is less than $100\,cm^{-1}$. The measurements were performed between 15000 and $50000\,cm^{-1}$ and the spectra were analyzed using peak-fit software. The purpose of the deconvolution of spectra is to confirm that both Ce(III) and Ce(IV) are present in the coatings independently of the oxidation state of the precursor salts.

2.4. Electrochemical characterization

Electrochemical test were conducted at room temperature in 3.5% NaCl solutions using an electrochemical unit (Solartron 1280B). Bare aluminum alloys were used for comparison. A three electrode cell was employed using a platinum wire of convenient area as counter electrode and a saturated calomel electrode (SCE, Radiometer Copenhague) as reference electrode. Potentiodynamic tests were conducted from the corrosion potential (Ecorr) to 0.4 V at a sweep rate of $0.002\,V\,s^{-1}$. Electrochemical impedance spectroscopy (EIS) was performed modulating 0.005 V rms in a frequency range of 20 kHz to 0.01 Hz. Impedance fitting was performed using a Zplot software [26].

3. Results

3.1. Physical and chemical characterization

All the sols obtained were transparent, colorless when using Ce(III) and red for Ce(IV) salts. Cerium doped silica coatings prepared 30 min after sol preparation appeared transparent and colorless when prepared with Ce(III) salt, and transparent faintly yellow with Ce(IV) salt. The thickness of coatings prepared with the Ce(III) salt was about 900 nm, and about 500 nm for Ce(IV) sols, due to the smaller solid concentration used in this sol. Although most films are homogeneous, defects were detected by optical microscopy in some Ce(III) coatings.

Fig. 1 shows the absorbance spectra of 90Si–10Ce coatings prepared with the Ce(IV) salt on glass substrates treated at 450 °C in three atmospheres and the band analysis of them. The deconvolution of the spectra showed two main bands centered around 32000 and $36500\,cm^{-1}$, assigned to Ce^{3+} and Ce^{4+} ions, respectively [27,28]. The semiquantitative evaluation of the Ce^{3+}/Ce^{4+} ratio, calculated taking into account the area

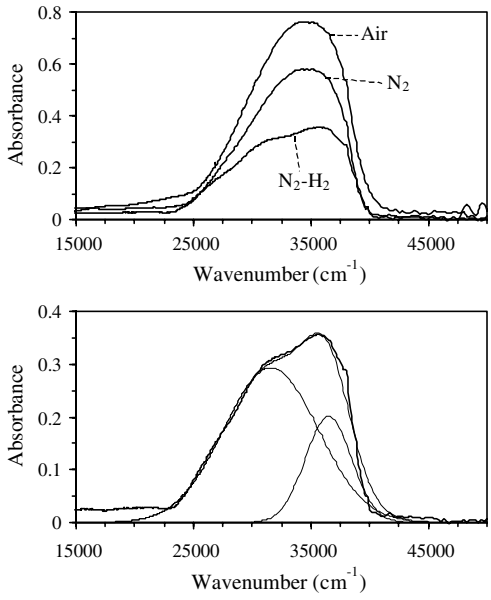

Fig. 1. Absorbance spectra of 90Si–10Ce coatings prepared with the Ce(IV) salt and treated at 450 °C: influence of the atmosphere treatment and deconvolution of the nitrogen–hydrogen treated coating spectrum.

of these bands, are 1.5, 1.8 and 2.9 for the samples treated in air, N_2 and $90N_2$–$10H_2$ atmospheres, respectively.

The absorbance spectra of the coatings prepared with the Ce(III) salt in the same atmospheres and the band analysis of the spectrum of the air treated coating are shown in Fig. 2. In this case, the band analysis of the spectra showed three main bands centered on 32200, 36300 and $42600\,cm^{-1}$. The $36300\,cm^{-1}$ band is assigned to Ce^{4+} ions as well as that appearing at $42600\,cm^{-1}$, while the absorption at $32200\,cm^{-1}$ is due to Ce^{3+} ions [27,28]. The semiquantitative Ce^{3+}/Ce^{4+} ratio for the 90Si–10Ce coating treated in air is 1.7. On the other hand the Ce^{3+}/Ce^{4+} ratios for the 95Si–5Ce coatings are 1.1, 1.5 and 2.1 for the samples treated in air, N_2 and $90N_2$–$10H_2$ atmospheres, respectively.

3.2. Electrochemical characterization

Corrosion potential for the bare aluminum alloy was −0.75 V after 7 min of soaking in 3.5% NaCl, meanwhile when the alloy is coated with the cerium containing coatings the potential is shifted cathodic reaching a constant −1.0 V after 10 min.

Figs. 3 and 4 show experimental frequency dependant impedance (EIS) collected for Ce(III) and Ce(IV) single and two layer coatings, and bare aluminum after 1 and 72 h of exposure in 3.5% NaCl solution. EIS change with exposure time is due to corrosion progression of the coated system.

Potentiodynamic polarization curves achieved for bare aluminum alloy showed a material in active dissolution with no signs of passivity in the potential range

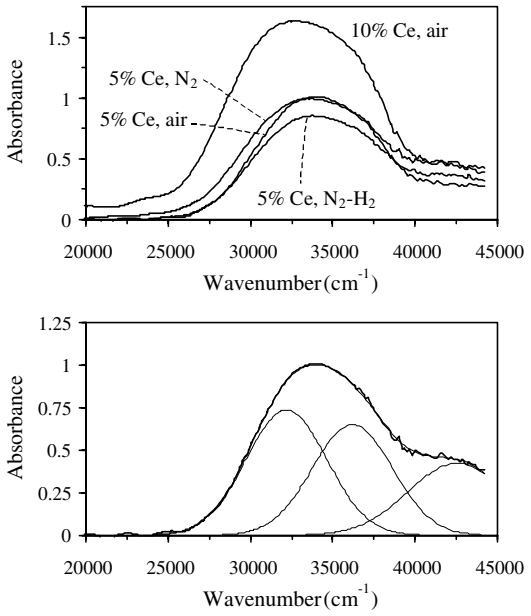

Fig. 2. Absorbance spectra of 90Si–10Ce and 95Si–5Ce coatings prepared with the Ce(III) salt and treated at 450 °C: influence of the atmosphere treatment and deconvolution of the air treated 95Si–5Ce coating spectrum.

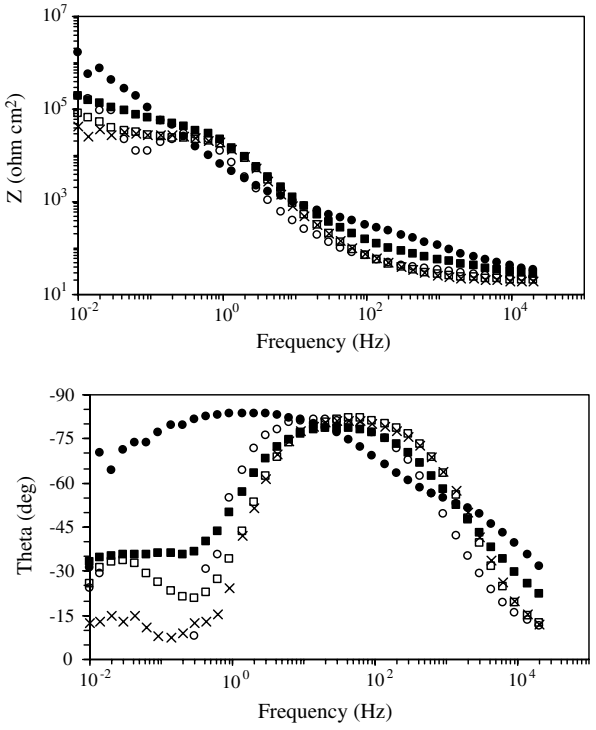

Fig. 3. Bode impedance plots of substrates coated with Ce(III) salt sol: one layer with NaCl immersion for 1 h (□) and 72 h (○), and two layers with NaCl immersion for 1 h (■) and 72 h (●). The curve of original aluminum with NaCl immersion for 1 h (×) is drawn for comparison.

under study. Potentiodynamic polarization curves measured on single and two layer Ce(IV) coatings after 1 h

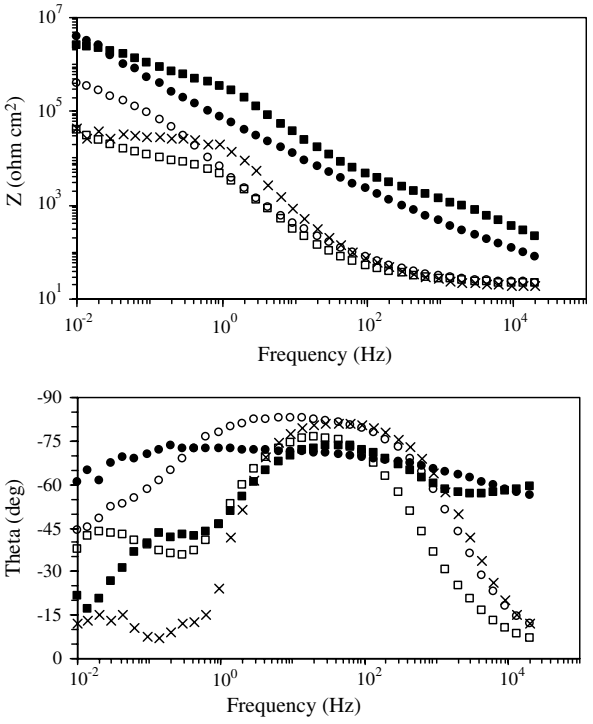

Fig. 4. Bode impedance plots of substrates coated with Ce(IV) salt sol: one layer with NaCl immersion for 1 h (□) and 72 h (○), and two layers with NaCl immersion for 1 h (■) and 72 h (●). The curve of original aluminum with NaCl immersion for 1 h (×) is drawn for comparison.

and 72 h of immersion and their comparison with bare aluminum alloy are shown in Fig. 5. Although both systems have a region of potentials of quasi stable current density after 1 h of immersion, the single layered system's density current is one order of magnitude larger than two layer systems, 3×10^{-7} to 4×10^{-6} Ampere (A) cm^{-2} for one layer and 10^{-8} to 10^{-7} A cm^{-2} for two layers. The potential breakdown, E_b, defined as the potential in which passivity breaks and current density increases in a monotonic way with potential, reach -0.71 ± 0.01 and -0.61 ± 0.015 V for the single layer and two layer coatings, respectively.

After 72 h of soaking in NaCl, Ce(IV) single layer coatings have smaller current densities and an increase of E_b (-0.32 ± 0.01 V) with respect to the initial immersion time, indicating an improved performance of the coating with time. Similarly, the Ce(IV) two layer coating had better properties than that at the initial stage of immersion: a very stable current density ($(1.91\pm1.25)\times10^{-7}$ A cm^{-2}) is maintained over a potential range, shifting the breakdown potential to -0.12 ± 0.01 V.

Polarization curves held on one layer Ce(III) coatings after 1 h of soaking are shown in Fig. 6(a). There is a range of potential, 0.17 ± 0.01 V, where the current remains unchanged. After 72 h of immersion, potential shifts anodic and the polarization curve resembles the aluminum one, showing no protection effect. The curves

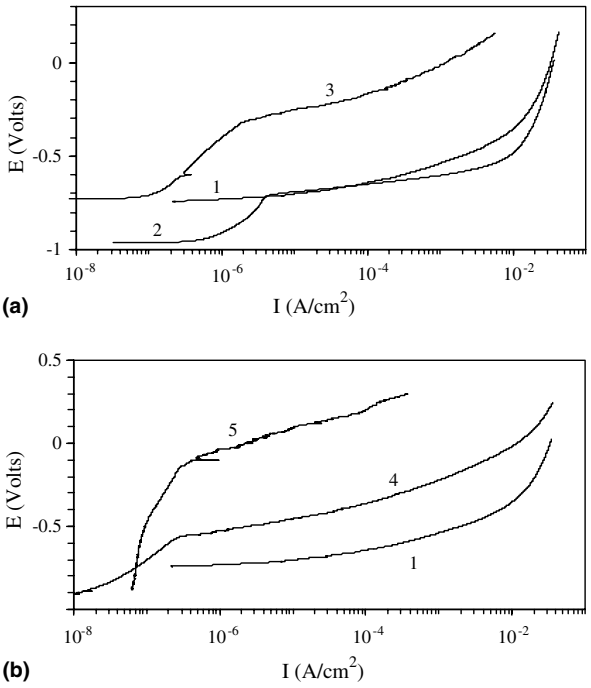

Fig. 5. Anodic polarization curves of substrates coated with the Ce (IV) salt sol: (a) one layer and immersion in NaCl solution for 1 h (curve 2) and 72 h (curve 3), and (b) two layers and immersion for 1 h (curve 4) and 72 h (curve 5). The curve of original aluminum with immersion in NaCl solution for 1 h (curve 1) is drawn for comparison.

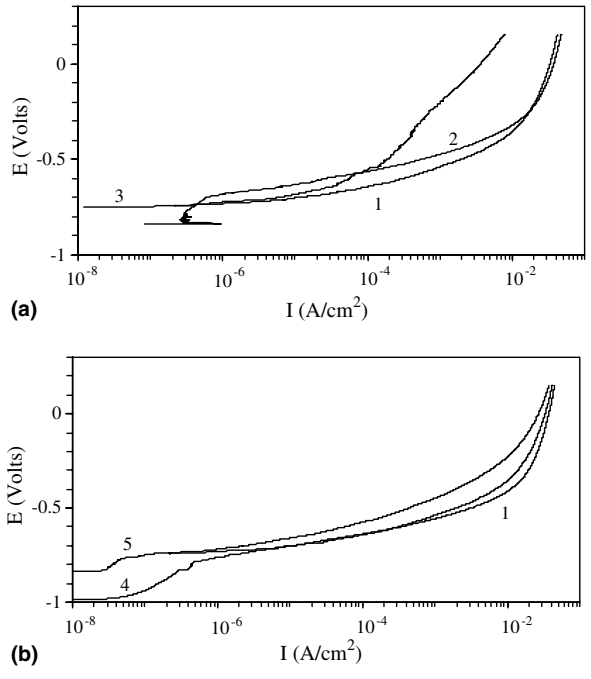

Fig. 6. Anodic polarization curves of substrates coated with the Ce(III) salt sol: (a) one layer and immersion in NaCl solution for 1 h (curve 2) and 72 h (curve 3), and (b) two layers and immersion for 1 h (curve 4) and 72 h (curve 5). The curve of original aluminum with immersion in NaCl solution for 1 h (curve 1) is drawn for comparison.

obtained for the two layer coating after 1 h of immersion in NaCl (Fig. 6(b)) had a range of current density varying from $(3.61 \pm 0.46) \times 10^{-8}\,A\,cm^{-2}$ to $(1.00 \pm 0.02) \times 10^{-6}\,A\,cm^{-2}$ in a potential range of 0.2 V. After 72 h of immersion, the potential shifts to more positive numbers, but current density remained constant at $(3.8 \pm 1.81) \times 10^{-8}\,A\,cm^{-2}$ in a narrow potential range (0.07 ± 0.01 V). Potential breakdown remained unchanged following after this point the features of the bare alloy.

4. Discussion

4.1. Physical and chemical characterization

Cerium is present in trivalent or tetravalent state by losing its two 6s electrons and one or both of its 4f electrons. The electron donation ability of Ce(III) facilitates the excitation of an electron from the 4f to the 5d shell, showing several characteristic broad bands in the UV region between 30 000 and 50 000 cm^{-1} nm, although the main absorption band is around 32 000 cm^{-1} [27]. The positions and intensities of these bands are affected by the metal ion site symmetry and the chemical species coordinated to the metal ion which in turn affects the ligand field. On the other hand, Ce(IV) favors charge transfer (CT) transitions from ligands to the ion, showing an intense band at around 43 000 cm^{-1} in most of glasses [27], although a band around 37 000 cm^{-1} has been also detected in some compositions [29–32]. The corrosion of Ce^{3+} and Ce^{4+} ions can be estimated by its affinity for oxygen through the standard free energy of formation of oxides. These energies for Ce_2O_3 and CeO_2 are -411.5 and -230.0 cal mol^{-1}, respectively, showing that Ce^{3+} has a larger potential as corrosion inhibitor [10].

All the coatings had bands from both Ce^{4+} and Ce^{3+} ions, although the kind of cerium salt used as precursor and the treatment atmosphere had an effect on the relative intensities. From the Ce^{3+}/Ce^{4+} ratio, we observed that Ce^{3+} is predominant over the Ce^{4+}, especially when using Ce(III) salt and reducing atmosphere. The more oxidant the atmosphere, the smaller is the redox ratio, showing that by changing the precursor and/or the treatment atmosphere it is possible to control the relative ratios of the ions.

On the other hand, we also observed that the redox ratio changes with the cerium content. As described for other redox pairs in glasses, such as Fe^{2+}/Fe^{3+} or Mn^{2+}/Mn^{3+}, the redox equilibrium of cerium is affected by the total content of the ion. Contradictory results have been reported for Ce^{3+}/Ce^{4+} ratio in different glass compositions [32]. In this work, the larger the concentration of cerium the larger is the ratio Ce^{3+}/Ce^{4+}, a similar effect as reported for Fe and Mn pairs.

Summarizing the UV–vis results, we concluded that independent from the cerium precursor, the cerium concentration, and the firing atmosphere, both Ce^{3+} and Ce^{4+} always are present in the coatings. Thus, for studying the electrochemical properties of cerium containing coatings, an unique concentration of 10% Ce with both precursors, and a single treatment condition in air have been applied.

4.2. Electrochemical characterization

The corrosion potential shifting to more negative numbers can be attributed to the property of cerium ions to be cathodic inhibitors against uniform and localized corrosion. It is achieved mainly by the decreasing of the oxygen reduction reaction [6]. This improvement is likely to the creation of a cerium oxide–hydroxide film that acts as a barrier to either the supply of oxygen to the metal or the supply of electrons from the metal surface. As a result of the reduction of cathodic sites, the overall corrosion rate is decreased [33].

To get more information about the corrosion feature occurring on the samples, EIS spectra were analyzed using equivalent electric circuits. In the simulation of impedance plots, the constant phase element (CPE) was used instead of an 'ideal' capacitor to explain the deviations from slope −1 in the modulus Bode plot. CPE can be described by the expression

$$Z_{\mathrm{CPE}} = \frac{1}{Y_0(\mathrm{j}\omega)^n} \tag{1}$$

with $-1 < n < 1$ [34]. In this equation, n is a coefficient associated to system homogeneity (being 1 for an ideal capacitor), ω is the frequency, and Y_0 is the pseudocapacitance of the systems that can be represented by

$$Y_0 = \frac{r\varepsilon\varepsilon_0 A}{d}. \tag{2}$$

In Eq. (2), ε_0 is the permittivity of free space, ε the dielectric constant of the surface film, d the thickness coating, A the exposed area and r the roughness factor [35]. Impedance spectra for the bare material after 1 h of immersion shows one time constant (Fig. 3). A simple equivalent circuit including a resistance and a constant phase element in parallel and the electrolyte resistance in series, can be adapted for the spectral fitting of the one time constant spectra (Fig. 7(a), Table 1).

Impedance results from one and two layer Ce(IV) coated samples after 1 h and 72 h of immersion are shown in Fig. 4. After 1 h of soaking, two time constants can be observed. That appearing at higher frequency is associated with the coating while the other one is referred to the metal alloy. The appearance of two maximum in the phase angle plot is related to the existence of defects in the coating. That means that the coating is acting as a 'leaky' dielectric, and showing that the electrolyte can access the surface through the defects and contact the substrate [36]. Ionic conductivity seems to diminish with exposure time, as observed when comparing the increase in phase angle below 1 Hz for samples with different immersion times. In the single layer coating some electrolytic conductivity is revealed as the phase angle decreases below 10 Hz. After 72 h of immersion, the phase angle plot does not have maximum for the two layer coating. That may mean that the film has a capacitive feature, although not fully capacitive, because the phase plot does not reach 90°. This change in the phase angle plot with the immersion time can be explained by the blocking of micro pores by corrosion products, followed by the reduction of the access of aggressive species to the metal interface. The slope in the low frequency range could also be associated to diffusion in solid phase. Nevertheless, according to the modeling, the controlling mechanism is charge transfer control indicating that charge transfer mechanisms are

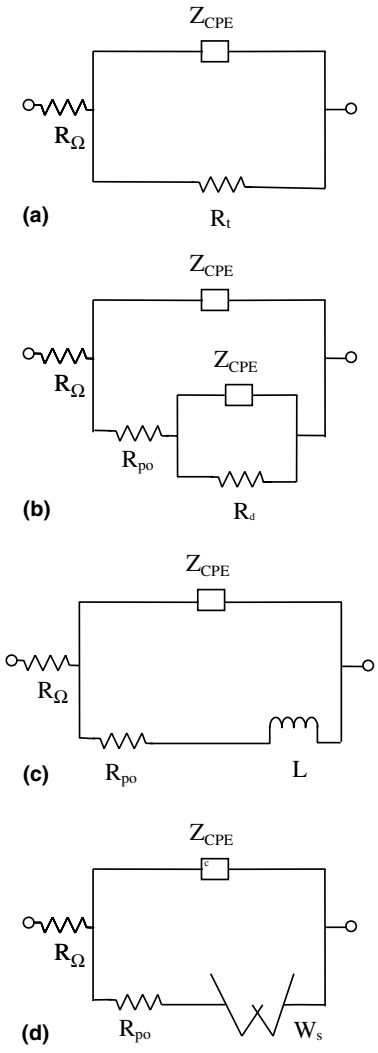

Fig. 7. Equivalent circuits used for fitting data of Figs. 3 and 4.

Table 1
Impedance parameters for one and two layer Ce(IV) coatings after 1 and 72 h of immersion in 3.5% NaCl

	$R_\Omega/\Omega\text{cm}^2$	$Y_{0c}/\Omega^{-1}\text{cm}^{-2}\text{s}^n$	n_c	$R_{po}/\Omega\text{cm}^2$	$Y_{0d}/\Omega^{-1}\text{cm}^{-2}\text{s}^n$	n_d	$R_t/\Omega\text{cm}^2$
Bare alloy 1 h immersion	21.2 ± 0.26				$7.44\times10^{-5}\pm1.40\times10^{-6}$	0.93 ± 2.9 × 10^{-3}	$1.23\times10^{4}\pm1.86\times10^{3}$
One layer Ce(IV) sol, 1 h immersion	22.56 ± 0.38	$1.11\times10^{-5}\pm2.69\times10^{-7}$	0.88 ± 3.81 × 10^{-3}	$2.46\times10^{4}\pm9.25\times10^{3}$	$9.42\times10^{-5}\pm6.87\times10^{-6}$	0.83 ± 3.71 × 10^{-2}	$1.106\times10^{5}\pm1.19\times10^{4}$
One layer Ce(IV) sol, 72 h immersion	23.44 ± 0.32	$6.51\times10^{-6}\pm9.62\times10^{-8}$	0.92 ± 2.4 × 10^{-3}	$3.12\times10^{5}\pm3.11\times10^{4}$	$1.18\times10^{-5}\pm2.68\times10^{-6}$	0.72 ± 9.8 × 10^{-2}	$1.74\times10^{6}\pm8.35\times10^{4}$
Two layers Ce(IV) sol, 1 h immersion	30.12 ± 2.51	$4.16\times10^{-7}\pm1.96\times10^{-8}$	0.77 ± 6.54 × 10^{-3}	$1.30\times10^{6}\pm1.21\times10^{5}$	$1.61\times10^{-6}\pm3.27\times10^{-8}$	0.97 ± 0.02	$1.56\times10^{6}\pm1.21\times10^{5}$
Two layers Ce(IV) sol, 72 h immersion	29.24 ± 1.21	$2.51\times10^{-7}\pm2.83\times10^{-8}$	0.75 ± 1.6 × 10^{-3}	$2.01\times10^{7}\pm2.07\times10^{6}$	$2.44\times10^{-7}\pm2.19\times10^{-9}$	0.99 ± 0.01	$3.06\times10^{7}\pm7.91\times10^{5}$

occurring slower than diffusion processes. The equivalent circuit shown in Fig. 7(b) was used to model the coated system and it consists of the following elements: R_Ω represents the electrolyte resistance, CPE_c is related with the non-ideal capacitance of the coating, R_{po} is the resistance of the electrolyte porosity, CPE_d is related with the non-ideal capacitance of the double layer of the bare metal, and R_t is the charge transfer resistance.

Table 1 shows the fitting of the data for the above named model. The increase in R_{po} we associate with the cerium inhibition effect and the plugging of corrosion products into the pores causing a decrease in the exposed area. The charge transfer resistance also increases due to the decrease of this area. The coating pseudocapacitance (Y_{co}) decreases with immersion time due to pore area decrease, and the exponent effect, n_{co}, increases probably due to surface smoothing.

Ce(III) sols applied as single layer have a different effect in the low frequency range with immersion time (Fig. 3). At the first stage of soaking, the system's response is similar to that obtained for the Ce(IV) coatings and the same equivalent circuit (Fig. 7(b)) can be used. R_{po} for Ce(IV) coating are larger than those of Ce(III) (Table 2) probably due to pre-existing defects in the Ce(III) coating, as was observed in the microscopy analysis (Fig. 8). After 72 h of immersion in sodium chloride, data reveal a capacitive component at high and medium frequencies followed by an inductive response at low frequencies. The equivalent circuit shown in Fig. 7(c) was used for data fitting. Tomcsanyi et al. [37] demonstrated that the inductive response may be caused by chloride ions that do not enter into the oxide film but are chemisorbed onto the surface oxide film formed on aluminum alloys, acting as a reaction partner aiding dissolution via the formation of oxychloride complexes. Fitting parameters are shown in Table 2.

The impedance data shown in Fig. 3 for the two layer Ce(III) coating after 1 h of immersion present a Warburg effect [34] we attribute to diffusion process taking place in the solid phase. This diffusion effect is probably more marked in the case of Ce(III) coatings than Ce(IV) ones because the former are thicker as explained in Section 3.1. The Warburg impedance and the CPE with n around 0.5 (the last known as 'infinite diffusion') [34] are used to model increasing ionic conductivity due to corrosion process occurring in the pores and increasing diffusivity into the pores. If the coating is thin (approximately below 2 μm), low frequencies will penetrate the entire thickness, creating a finite length Warburg element. Only if the material is thick enough so that the lowest frequencies do not penetrate the layer, it is interpreted as infinite (Eq. (3)) [26]

$$Z_w = \frac{R_{DO}}{(jT\omega)^n}\tanh(jT\omega)^n. \quad (3)$$

Table 2
Impedance parameters for one layer Ce(III) coating after 1 and 72 h of immersion in 3.5% NaCl

	$R_g/\Omega cm^2$	$Y_{0c}/\Omega^{-1} cm^{-2} s^n$	n_c	$R_{po}/\Omega cm^2$	$Y_{0d}/\Omega^{-1} cm^{-2} s^n$	n_d	$R_t/\Omega cm^2$	L
One layer Ce(III) sol, 1 h immersion	21.02 ± 0.25	5.14×10^{-6} ± 8.11×10^{-8}	0.94 ± 2.4 × 10^{-3}	2.71×10^4 ± 3.72×10^2	1.39×10^{-4} ± 6.2×10^{-6}	0.97 ± 2.11 × 10^{-2}	7.65×10^4 ± 3.65×10^3	
One layer Ce(III) sol, 72 h immersion	25.65 ± 1.13	5.94×10^{-6} ± 1.89×10^{-7}	0.87 ± 5.5 × 10^{-3}	3.95×10^4 ± 2.37×10^4				2.44×10^4 ± 1.11×10^3

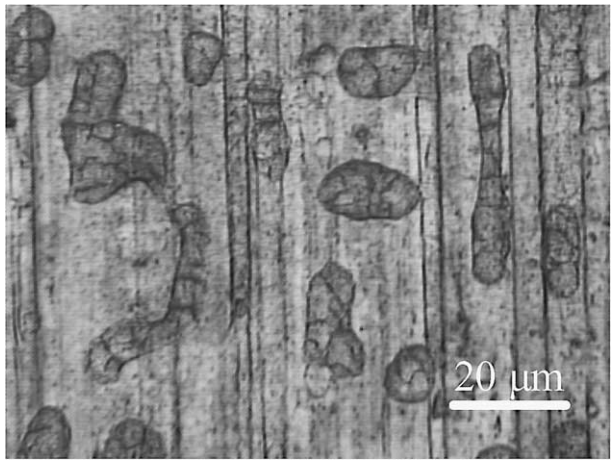

Fig. 8. Optical microscopy photograph of a 90Si–10Ce coating prepared with the Ce(III) salt showing the presence of cracks.

In Eq. (3), R_{DO} is associated with solid phase diffusion and T is related to diffusion coefficient and porous length.

The impedance can be fitted by a circuit that includes a finite Warburg element (Fig. 7(d)). The phase angle decreases at low frequencies not reaching zero, which we suggest is due to the presence of pores in the outer part of the coating and diffusion effects inside them [38]. After 72 h of immersion porosity and/or defects seemed to be blocked with corrosion products making diffusion more difficult and increasing corrosion resistance of the sample. Thus, fitting results shows that both R_{po} and R_{DO} (resistance associated to diffusion in solid phase) increase, increasing the resistance into the pores and the diffusion resistance of the ionic species in solid phase or the diffusion of oxygen or anions into the coating. Fitting parameters are given in Table 3.

The electrochemical parameters derived from the polarization curves together with the EIS results, revealed the protective role of Ce(IV) coatings that persists with immersion time, a protective effect that is improved for the two layer coating system. Ce(III) coatings can only reach a protective feature when the coating is made in two steps, probably due to sealing of pre-existent porosity or defects.

Sol–gel coatings used as protection of different metals against corrosion do not usually improve with the immersion time. In fact, depending on the composition and structure of the coating (totally inorganic or hybrid), the electrolytic medium and the soaking time, deterioration of the coatings occurs, permitting the contact of the electrolyte with the substrate and thus decreasing the protector effect [21–24]. However, the application of sol–gel coatings in this work leads to an improvement in the corrosion protection. The increase of immersion time probably leads to the release of cerium in the defects of the coatings. Then, cerium produces insoluble hydroxides when it reacts with

Table 3
Impedance parameters for two layer Ce(III) coating after 1 and 72h of immersion in 3.5% NaCl

	$R_\Omega/\Omega\,cm^2$	$Y_{0c}/\Omega^{-1}cm^{-2}s^n$	n_c	$R_{po}/\Omega cm^2$	$R_{DO}/\Omega cm^2$	n_d	T
Two layers Ce(III) sol, 1h immersion	30.89 ± 1.07	$5.18 \times 10^{-6} \pm 2.08 \times 10^{-7}$	$0.87 \pm 6.1 \times 10^{-3}$	$6.15 \times 10^4 \pm 5.7 \times 10^3$	$1.25 \times 10^5 \pm 2.31 \times 10^4$	0.58 ± 0.049	11.41 ± 2.91
Two layers Ce(III) sol, 72h immersion	30.16 ± 1.41	$5.32 \times 10^{-6} \pm 1.72 \times 10^{-7}$	$0.89 \pm 5.7 \times 10^{-3}$	$2.73 \times 10^6 \pm 1.13 \times 10^5$	$8.39 \times 10^5 \pm 4.02 \times 10^4$	0.99 ± 0.01	2.91 ± 0.029

hydroxyl groups from cathodic reactions [10,12,13]. These hydroxides together with corrosion products decrease the cathodic current and, therefore, reduces the overall corrosion rate. Future work is in progress to study the mechanism proposed using coatings with different cerium concentrations and thickness.

5. Conclusions

Cerium doped silica sol–gel coatings on glass and aluminum substrates were obtained using Ce(III) and Ce(IV) salts. The UV–vis spectra obtained with coatings prepared on glass substrates showed that both Ce^{3+} and Ce^{4+} are always present, although the kind of cerium salt used as precursor and the treatment atmosphere affect the relative intensities.

The electrochemical properties of the system demonstrated the protective role of the cerium when incorporated in sol–gel coatings, both in single and two layer films. The improvement of coating performance in time is related to the plugging of corrosion products into the pores and the inhibition effect of cerium, causing a decrease in the exposed area and reducing cathodic current.

Acknowledgment

This work has been partially financed by the CYTED project VIII.9 and the CICYT Project MAT2003-05902.

References

[1] A.-M. Moreno (Ed.), World Aluminium: A Metal Bulletin Databook, Metal Bulletin Books, Surrey, England, 2001.
[2] Metals Handbook, ninth ed., Non-Ferrous Alloys and Pure Metals, vol. 2, 1997.
[3] C. Kammer (Ed.), Aluminium Handbook, Aluminium-Zentrale, Düsselfod, 1999.
[4] R.T. Foley, Corros. Sci. 42 (1986) 277.
[5] W.J. Wittke, Met. Finish. 87 (1989) 24.
[6] M. Bethencourt, F.J. Botana, J.J Calvino, M. Marcos, M.A. Rodriguez-Chacon, Corros. Sci. 40 (1998) 1803.
[7] S. Bernal, F.J. Botana, J.J. Calvino, M. Marcos, J.A. Pérez-Omil, H. Vidal, J. Alloy Compd. 225 (1995) 638.
[8] M.A. Arenas, M. Bethencourt, F.J. Botana, J. de Damborenea, M. Marcos, Corros. Sci. 43 (2001) 157.
[9] M.A. Arenas, A. Conde, J.J. de Damborenea, Corros. Sci. 44 (2002) 511.
[10] Y.C. Lou, M.B. Ives, Corros. Sci. 37 (1995) 145.
[11] Y.C. Lou, M.B. Ives, Corros. Sci. 34 (1993) 1773.
[12] W.G. Fahrenholtz, M.J. O'Keefe, H. Zhou, J.T. Grant, Surf. Coat Technol. 155 (2002) 208.
[13] F. Mansfeld, S. Lin, S. Kim, H. Shih, J. Electrochem. Soc. 137 (1990) 78.
[14] A.E. Hughes, R.J. Taylor, B.R.W. Hinton, L. Wilson, Surf. Interface Anal. 23 (1995) 540.
[15] B.R.W. Hinton, J. Alloy Compd. 180 (1992) 15.

[16] B.R.W. Hinton, D.R. Arnott, N.E. Ryan, Met Forum 7 (1984) 211.
[17] M.W. Kendig, R.G. Buchheit, Corrosion 59 (2003) 379.
[18] B.R.W. Hinton, L. Wilson, Corros. Sci. 29 (1989) 967.
[19] P. Innocenzi, M.O. Abdirashid, M. Guglielmi, J. Sol–Gel Sci. Technol. 3 (1994) 47.
[20] M.A. Villegas, M. Aparicio, A. Duran, J. Non-Cryst Solids 218 (1997) 146.
[21] O. de Sanctis, N. Pellegri, A. Durán, J. Non-Cryst Solids 121 (1990) 338.
[22] J. de Damborenea, N. Pellegri, A. Durán, J. Sol–Gel Sci. Technol. 4 (1995) 239.
[23] A. Morales, A. Durán, J. Sol–Gel Sci. Technol. 8 (1997) 451.
[24] P. Galliano, J. de Damborenea, M.J. Pascual, A. Durán, J. Sol–Gel Sci. Technol. 13 (1998) 723.
[25] M.A. Sainz, A. Duran, J.M. Fernandez, J. Non-Cryst Solids 121 (1990) 315.
[26] Zplot for Windows, Electrochemistry, Impedance Software Operating Manual, Part 1, Scribner Ass. Inc., Southern Pines, NC, 1998.
[27] G.U. Zhenan, J. Non-Cryst Solids 52 (1982) 337.
[28] H. Ebendorff-heidepriem, D. Ehrt, Opt. Mater. 15 (2000) 7.
[29] R. Reisfeld, H. Minti, A. Patra, D. Ganguli, M. Gaft, Spectrochim. Acta Part A 54 (1998) 2143.
[30] S. Aubonnet, C.C. Perry, J. Alloy Compd. 300–301 (2000) 224.
[31] A. Patra, D. Kundu, D. Ganguli, J. Sol–Gel Sci. Technol. 9 (1997) 65.
[32] A. Paul, R. Douglas, Phys. Chem. Glasses 6 (1965) 212.
[33] L.S. Kasten, J.T. Grant, N. Grebasch, N. Yoevodin, F.E. Arnold, M.S. Donley, Surf. Coat Technol. 140 (2001) 11.
[34] CMS100 Systems, Operator's Manual Addendum, Changes for CE Compliance, Gamry Instruments, Inc., PA, USA, 1996.
[35] C. Liu, Q. Bi, A. Leyland, A. Matthews, Corros. Sci. 45 (2003) 1257.
[36] C. Liu, Q. Bi, A. Leyland, A. Matthews, Corros. Sci. 45 (2003) 1243.
[37] L. Tomcsanyi, K. Vaga, I. Bartik, G. Horanyi, E. Maleczki, Electochim. Acta 34 (1989) 855.
[38] M. Metikos-Hukovic, E. Tkalcec, A. Kwokal, J. Piljac, Surf. Coat Technol. 165 (2003) 40.